Effect of asymmetrical orifice inlet geometry on spray kinematics and development

(article starts on next page)

Full length article

Effect of asymmetrical orifice inlet geometry on spray kinematics and development

Mohammad Nikouei [a,b,*], David Sedarsky [a]

[a] *Chalmers University of Technology, Gothenburg, Sweden*
[b] *Scania CV AB, Södertälje, Sweden*

A B S T R A C T

In diesel engines, fuel injection has a commanding effect on combustion. Thus studying diesel spray characteristics is beneficial for controlling and improving diesel combustion. However, information on diesel spray characteristics, especially those governed by injector needle lift, is lacking. This study investigates the near-nozzle spray kinematics for particular nozzle geometries over a range of injection pressures. The nozzles used in this research include a single-hole off-axis nozzle and a two-hole nozzle with deviated orifices. This study aims to observe the effect of asymmetrical orifice inlet on the spray kinematics and describe how sensitive they are to the injection pressure. First, we applied double-pulses time-gated ballistic imaging to obtain well-defined spray/gas interfaces. Then, by tracking these interface structures, we obtained spray kinematics. The results show that the two-hole nozzle generates slower sprays than the single-hole nozzle at the beginning of injection. However, the velocity differences between these sprays become less significant as the sprays develop to a quasi-steady state. In addition, the velocity diagrams show that the instabilities cause the flow to experience significant velocity alterations at the beginning of the injection. Moreover, we observed that the nominal spray axis shifts towards the sharper orifice inlet edge, which will affect the spray targeting. Finally, the injection pressure seems to have minimal effect on the spray profile, but it certainly changes spray evolution timing and shortens the transient phase.

1. Introduction

In Compression Ignition (CI) engines, fuel injection has a commanding effect on combustion. In other words, controlling injection parameters can influence combustion products. However, this is not simple since the number of parameters affecting fuel spray characteristics is relatively large. In addition, these parameters are not independent. Hence, interactions between injection parameters make it complicated to find the optimum configuration for different operating conditions. Some sources address the effect of parameters such as injection pressure [1–3] and temperature [4] on spray characteristics. In addition, experiments with different fuels show that the fuel properties can also affect spray behavior [2,5,6], mainly due to their physical properties, such as viscosity and boiling temperature. Furthermore, studies show that the design of nozzle geometry plays an essential role in spray break-up [6,7] and even the combustion products [8]. However, the nozzle geometry itself consists of several parameters such as hole diameter, orifice length, orifice angle, edge roundness, and conicity level. Moreover, if the cross-section of the orifice exists in shapes other than a circle (e.g., elliptical shape [9]), even more parameters

will be involved. Although these geometrical parameters have been studied earlier [10,11], however, little attention has been paid to the effect of asymmetrical inlet geometries on spray behavior. For this purpose, we have selected two specially built nozzles to investigate the effect of asymmetrical inlet geometries. These asymmetries are usually present in conventional multi-hole injectors used in production. The asymmetry level of the orifice inlet changes by orifice position or its inclination angle. In addition, measurements of penetration length over time [12] show a relation between orifice angle and penetration velocity. Therefore, the study of spray velocity profile in angled orifices would be complementary. Hence, we intend to explain spray behavior by measuring and analyzing near-field spray velocity profile characteristics. According to Zama et al. [13] the spray post-impingement behavior depends on its velocity profile prior to impingement because velocity can influence the heat transfer mechanism. Accordingly, it is possible to predict spray behavior by near-field velocity profile.

Various methods have been used to measure spray velocity for different spray regions and Sedarsky et al. [14] have listed the advantages and disadvantages of some of these methods including LCV, LDV, PIV,

---

* Corresponding author.

E-mail address: mohammad.nikouei@scania.com (M. Nikouei).

Abbreviations

ASOI	After the Start Of Injection
ASP	Average Spray Profile
BBO	Barium Borate
BI	Ballistic Imaging
CI	Compression Ignition
CS_2	Carbon di Sulfide
HSOI	Hydraulic Start Of Injection
ICCD	Intensified Charge-Coupled Device
ICV	Image Correlation Velocimetry
LCV	Laser Correlation Velocimetry
LDV	Laser Doppler Velocimetry
OA	Off-Axis nozzle
OKE	Optical Kerr Effect
PIV	Particle Image Velocimetry
SH	Single-Hole, on-axis nozzle
SOI	Start of Injection
TH − A	Two-Hole nozzle-orifice A
TH − B	Two-Hole nozzle-orifice B
TH	Two-Hole nozzle
XPI	eXtra high Pressure Injection

and ICV. However, the presence of ultra-dense liquid core in the near-field does not allow the implementation of most of the mentioned techniques, especially the PIV [15]. The PIV method requires tracking particles while no particle can be detected in the near-field, since the dense liquid core obscures them. Hence, we only track the spray interfaces as a solution to measure near-field spray kinematics. This approach requires clear and distinguishable spray structures. In order to obtain well-defined structures, we apply time-gated ballistic imaging [16], which is a line-of-sight imaging method. This imaging setup can reduce multiple-scattering noises and provide a high-resolution spray interface. This method was initially used for medical applications, but it was also used for study spray after a while.

Similar to Sedarsky et al. [14], we have applied cross-correlation on double-exposure images to measure the gas/liquid interface's velocity. However, in the current work, we have focused on the effect of specific inlet geometries on spray kinematics. In order to measure fluid interface velocity, we need pairs of images to apply correlation and extract displacement vectors. Therefore, we apply two synchronized laser pulses to collect a pair of consecutive images of the same injection event. In Section 2, we have described image acquisition and experimental setup details. Section 2.5 provides data processing and analysis and explains how we extracted velocity data. Finally, Section 3 shows the results and velocity profiles, followed by a discussion about how the spray behavior and velocity profiles affected by inlet geometries and injection pressure.

2. Experimental setup

2.1. Image acquisition

As mentioned earlier, the main objective of this research is to measure and compare near-field sprays generated by asymmetrical orifice inlet geometries. At a very short distance to the nozzle, no or just a little break-up occurs, and therefore, it is challenging to identify and track seeding particles. On that account, one can suggest tracking fluid interface instead of seeding particles; however, this solution requires high spatial resolution images with well-defined structures. The time-gated ballistic imaging method filters noise from multiple scattering and can produce high-resolution images to identify and accurately trace

fluid interface structures. However, the ballistic imaging setup requires high-power ultra-short laser pulses.

For this study, we have used two regenerative amplifiers seeded by a common Ti-Sapphire oscillator. The output beams consist of ultra-short (femtosecond) pulses with the wavelength of 800 nm. Pulse emission frequency is 1 kHz, which is insufficient to capture consecutive images of a whole injection event. Therefore, we use two light sources that are aligned and synchronized together. As Fig. 1 illustrates, laser pulses are divided into two parts using a beam splitter. The first portion is used as the light source for imaging, while the other portion activates birefringence in a carbon disulfide (CS_2) cell. We have evaluated activation period for CS_2 to be slightly less than 2 ps. During this period, the polarization of transmitted photons rotates by 90°. We place the CS_2 cell between two polarizers, which are perpendicular to each other. With this configuration, the photons passing through the first polarizer can only pass through the second polarizer when the CS_2's birefringence is active. This configuration allows only the photons with the least interaction with spray to reach the detector and filters the rest of the multiple scattering photons. When the imaging beam is transmitted through a Barium Borate (BBO) Crystal, its frequency is doubled, minimizing the interaction between the imaging and switching beams. This configuration is known as co-linear ballistic imaging [17].

We have used an ICCD camera featuring double imaging function (PI-Max 4) for capturing image pairs. The dwell time between each shot should be set as short as possible to retain the spray structure, but it should also be long enough to allow the sensor phosphor to decay. The trade-off between these requirements showed that 560 ns is suitable for this application. The resolution of the camera sensor is 1024 × 1024 pixels, and the spatial resolution of the optical setup is measured to be 8.33 μm per pixel length.

2.2. Hardware

In addition to the optical setup, the test rig includes a fuel supply system, a constant volume chamber, and a control system. The fuel pump is driven by an electric motor, delivering fuel to the injector with pressures as high as 2400 bar. The fuel supply system has two fuel rails equipped with one pressure sensor on each rail to create a closed-loop control of the fuel pressure. In addition, the fuel passes through two filters before entering the fuel rails. Finally, this system has been equipped with two heat exchangers operated by tap water to keep the fuel temperature constant. The injections occur in a constant volume chamber. This chamber is designed for ambient temperature conditions and can be pressurized up to 30 bar.

The control system consists of a signal generator and a pulse picker device. The pulse picker can generate signals with the same phase of the laser pulse as soon as the user triggers it. This pulse is then used as the input to the signal delay generator device. Finally, we adjust appropriate time delays on this device to trigger the camera and the injector driver independently at the right moments.

The injectors used in this study are the XPI (eXtra high-Pressure Injector), designed and developed by Cummins. These injectors are side-fed, and due to the geometrical constraints, there is no choice but to install the injector diagonally on the chamber. In this setup, the angle between the injector and the horizontal axis is 21°. We perform experiments on three prototype nozzles with different geometries to study the effect of inlet geometry on near-field spray velocity. As it illustrated in Fig. 2, one of the nozzles is a normal single-hole nozzle and its orifice axis is located in the middle of the sac. The second nozzle is also a single-hole but with an off-axis orifice. Finally the last one is a two-hole nozzle with deviated orifices in which their umbrella angle is 146°. Fig. 2 illustrates the schematic half section view of these nozzles. This Figure shows how the curvature of the sac volume and the position of orifices can create asymmetrical geometry at the orifice inlet and outlet. Therefore, it is evident that conditions would be different for the flow reaching either side of the orifices in the latter two cases. Table 1
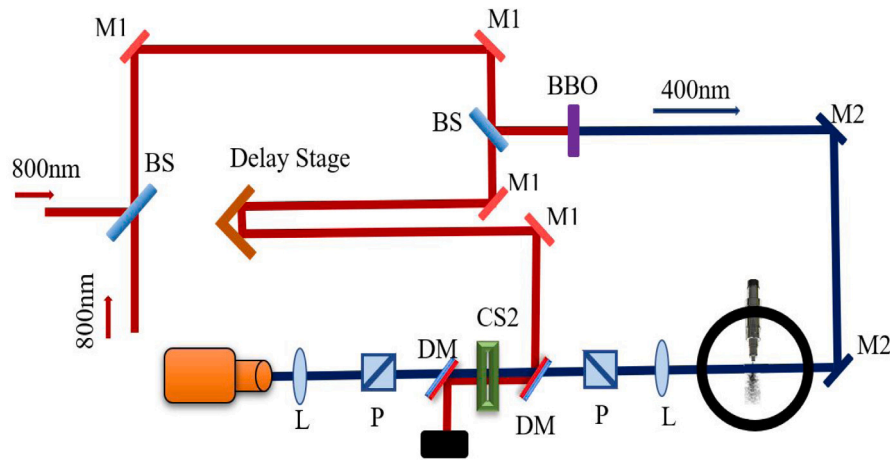
Fig. 1. A schematic view of image acquisition system configuration. M1: 800 nm mirror, M2: 400 nm mirror, BS: beam splitter, P: polarizer, L: lens, DM: dichroic mirror.
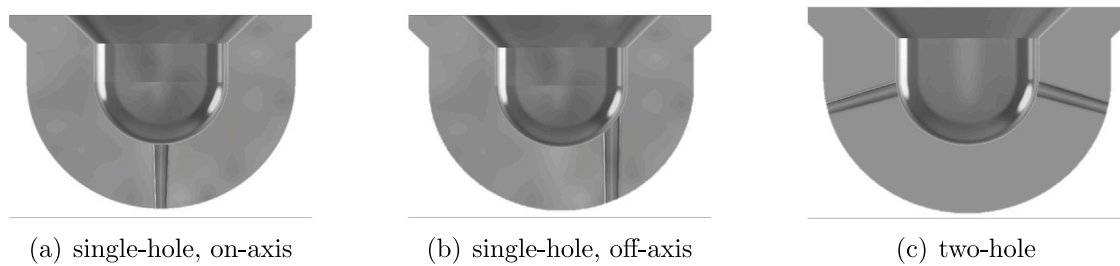

(a) single-hole, on-axis

(b) single-hole, off-axis

(c) two-hole

Fig. 2. Schematic view of nozzle geometry.

Table 1
Nozzles specifications.

Nozzle	SH	OA	$TH-A$	$TH-B$
Outlet diameter [μm]	178	224	205	200
Inlet diameter [μm]	198	234	224	219
Orifice length [mm]	1	0.7	1	1
k-factor	2	1.4	2	2
Hydro-grinding level [%]	30	15	15	15

Table 2
Experimental conditions.

Parameter	Value	Unit
Rail pressure	800, 1200, 1600	bar
Back pressure	atm	–
Ambient temperature	294	K
Injection duration	2	ms

indicates specifications for each orifices; To distinguish the orifices of the two-hole nozzle, we label them with letters A and B. In addition, we use SH, OA and TH abbreviations for referring to the single-hole on-axis, off-axis and the two-hole nozzles, respectively.

2.3. Experimental conditions

A high-pressure fuel pump continuously supplies commercially available diesel fuel to the injector over a range of pressures. This pump is equipped with a heat exchanger to cool the fuel with open-loop tap water and keep the fuel temperature constant. We performed experiments with 800, 1200, and 1600 bar of rail pressure in this work. Table 2 shows the other details about the experimental conditions.

2.4. Experiment procedure

We set the injector triggering signal to 2 ms. Since laser pulses frequency is 1 kHz (one pulse per millisecond), we cannot take more than a pair of images per injection event. Therefore, we estimate velocities based on a statistical average of several injection events to cope with this limitation. For this purpose, we took at least 150 image pairs for each discreet time instants after the start of injection. Studies include time instants from 20 to 50 μs after Hydraulic Start Of Injection (HSOI) with increments of 10 μs. HSOI is the reference time and it is unique for each orifice. HOSI is described as the moment when the fuel is on the verge of leaving the nozzle. In order to get this time instant, we take a bunch of images with 1 μs of intervals just before emergence of fuel until it comes out of the nozzle. At the initial stage of spray penetration, spray penetration grows linearly with the time because the momentum exchange rate between the liquid column and surrounding air is close to zero [18]. Therefore, during the very early stage of injection, the velocity of spray penetration is calculated based on spray penetration length. Accordingly, the relative timing for penetration equal to zero is obtained, and we set other time intervals according to this point.

2.5. Data processing

As stated earlier, this study aims to obtain the spray velocity based on tracking the displacement changes of the resolved spray structures. Here, we define these structures as in-focus concentrated liquid structures mainly seen at the spray's edge. In addition, droplets larger than 25 μm can also be considered as such structures that are confined to the 50 μm object plane created by the light collecting optics.

All images undergo normalization and background subtraction. Next, we rotate images to align the orifice axis with the vertical axis for all cases. In some cases, we also flipped images horizontally so that the sharper edge of the orifice lays on the left side of the vertical axis.
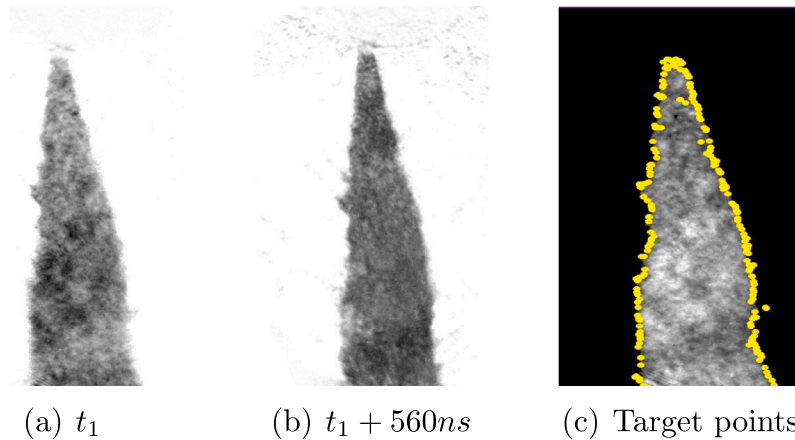
(a) t_1 (b) $t_1 + 560ns$ (c) Target points

Fig. 3. Example of one image pair taken with a time difference of 560 ns and distribution of target points.
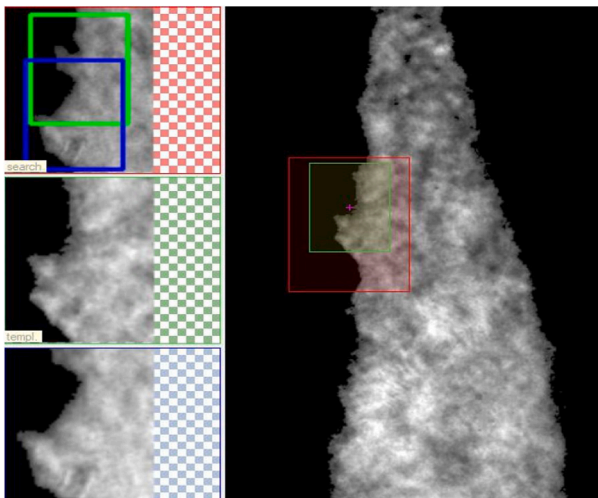

Fig. 4. An example of spray tracking. On the left side, green square shows the position of the template in the first image and the blue square is the matched template from the second image. The red box indicates the search field. (For interpretation of the references to color in this figure legend, the reader is referred to the web version of this article.)

Performing a fast normalized cross-correlation on image pairs provides displacement vectors across the spray periphery. For this purpose, the spray edge is detected first by the Sobel algorithm. Then, we randomly distribute several target points on the spray edge (Fig. 3). The information around each target point, including the pattern and intensity, is captured in the next step. This information is correlated within a certain distance from the same coordinates on the second image. Finally, all correlations undergo a validation test, which is done based on the correlation coefficient or the percentage of similarity as well as the maximum and minimum anticipated values for displacement. Fig. 4 visually explains this process, that yields displacement vectors of the spray periphery on a 2D plane over a specific time. In the last step, we calculate the velocity magnitude of each point assuming that the displacement in the direction normal to the plane is equal to the displacement in the horizontal direction.

Since there are shot-to-shot variations in spray profile, therefore, we extract velocity data for Average Spray Profile (ASP) at each time instant and injection pressure. For each coordinate on the ASP (Fig. 5(a)), mean velocity is calculated by averaging the velocity data available in the vicinity (8 × 8 pixels) of the respective point. The source of this velocity data is velocity vectors extracted from all individual image pairs at respective time instant and injection pressure (Fig. 5(b)).

3. Results and discussion

The main results of the experiments are statistical velocity maps of the near-field spray periphery. We have combined these velocity maps in Figs. 7, 8 and 9. In these images, each column represents the time instant after HSOI, and each row belongs to particular injection pressure. In each plot, a set of points indicate the approximate spray interface at the corresponding time instant, which mostly involved with air entrainment. The vertical and horizontal axes show the coordinates of each point relative to the nozzle tip, and the color of each point indicates the average spray velocity magnitude around that point. In the image processing stage, we have rotated or flipped all the images so that all orifice axes coincide with the vertical axis, and the sharper edge of the orifice inlet has been placed on the left side.

This research is based on the statistical measurement of spray kinematics. In addition, the spray has a variable nature, and we have witnessed shot-to-shot variation. Therefore, it is necessary to test the reliability of the results using statistical methods. As mentioned earlier, we sampled at least 150 image pairs per injection case, resulting in 100 to 200 validated velocity vectors near (within 8 × 8 pixels) each local target point. Hence, each mean velocity value has been obtained by a variable amount of samples and standard deviations. Using Eq. (1) and the t-distribution table, we can determine the confidence interval of the actual mean value for any points on the spray edge based on the available sample population and their standard deviation.

$$\bar{y} - t_{\alpha/2, n-1}(S/\sqrt{n}) \leq \mu_0 \leq \bar{y} + t_{\alpha/2, n-1}(S/\sqrt{n}), \tag{1}$$

where $\bar{y}$ is the sample mean, μ_0 is the actual mean value, S is the sample's standard deviation for the sample size of n, and α determines uncertainty level.

Fig. 6 shows velocity distribution diagrams for two particular cases and the confidence intervals for corresponding cases. For each target point on the spray periphery, we calculated the confidence interval and deviation from the actual mean with the certainty of 95%. The diagrams show that at 800 bar, the measured mean values look convergent with a maximum deviation of ±12 m/s. However, this value is slightly larger for the case with 1600 bar injection pressure and is equal to ±18 m/s. In addition, higher injection pressure creates more turbulence and more shot-to-shot variation. Therefore, it is evident that the standard deviation is higher at 1600 bar.

3.1. Nozzle geometry

These images show that the velocity magnitudes of TH nozzle's sprays are considerably lower than for the OA. According to continuity in fluids, the increase in cross-sectional area under constant pressure is
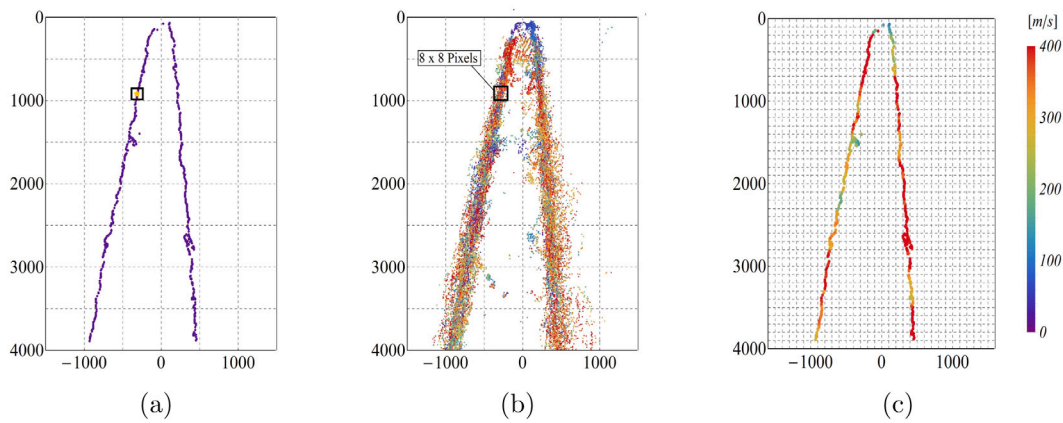
Fig. 5. Example of one image pair taken with a time difference of 560 ns and distribution of target points. (a) Target point representing average spray profile, (b) all measured velocity data, (c) average velocity profile on average spray profile.
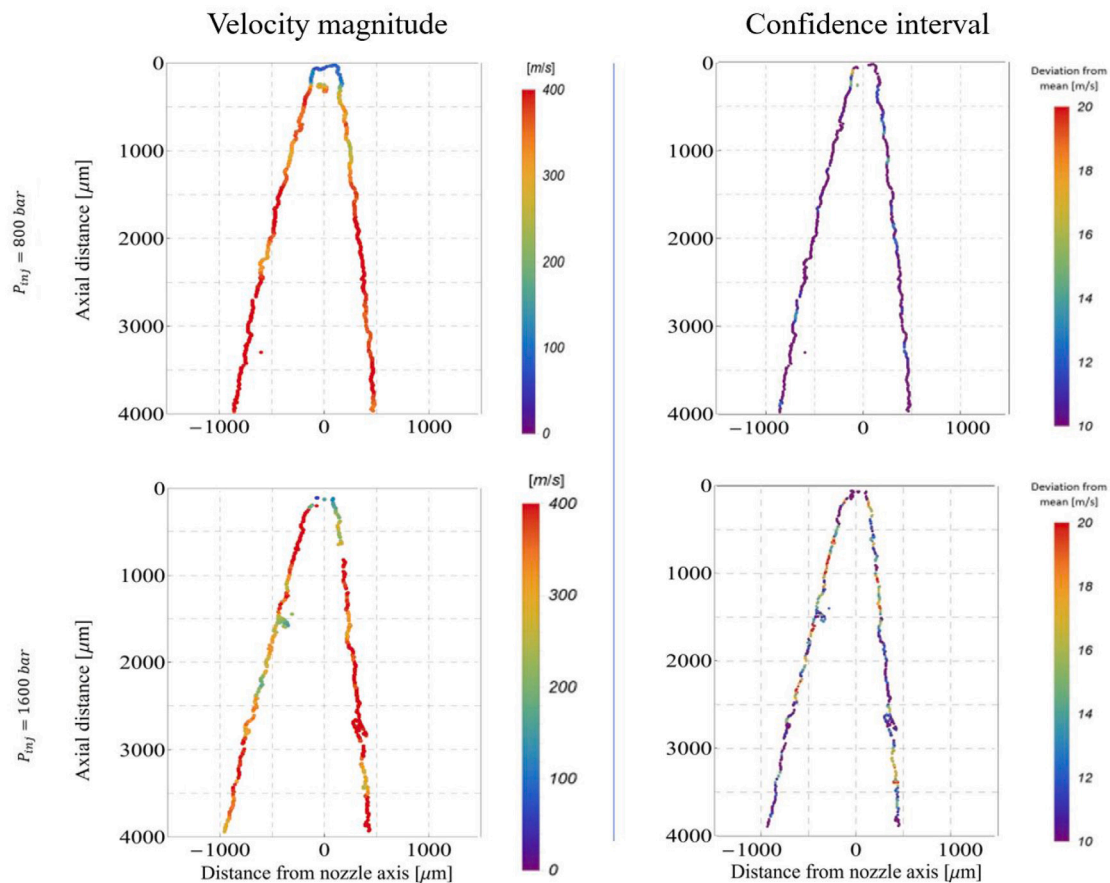

Fig. 6. Confidence intervals for the actual mean values for two injection pressures for nozzle OA at 800 μs ASOI.

inversely proportional to the velocity of the fluid; therefore, it seems that the larger total cross-sectional area at the TH nozzle outlet lowers the velocity in both TH nozzle's orifices. However, the difference between velocity magnitudes becomes less significant at the quasi-steady state (800 μs). Therefore, the position of the injector needle seems to be important in this case. We assume that the needle is still at a low lift at the beginning of the injection, which delivers a very low incoming flow rate to the sac volume. On the other hand, the total cross-sectional area of TH nozzle is larger than the OA. Therefore, it will take longer for the TH nozzle to recover its sac pressure.

Fig. 10 shows the distribution of the spray velocity at specific distances from the nozzle tip at two time stages with the injection pressure of 1600 bar. The deceleration of spray at 40 μs after the start of the injection is evident for all three orifices. According to the diagrams, on the positive X-axis, the velocity goes down from 420 m/s (at 1 mm) to about 380 m/s (at 3 mm) for the OA nozzle. However, the highest deceleration can be seen for the TH-A orifice, so that velocity reduction from 400 m/s to 150 m/s occurs within a 2 mm distance. Nevertheless, deceleration is insignificant at 800 μs within the first 3 mm downstream. Perhaps less interaction with the surrounding air and higher interaction with the liquid core could be a possible reason.
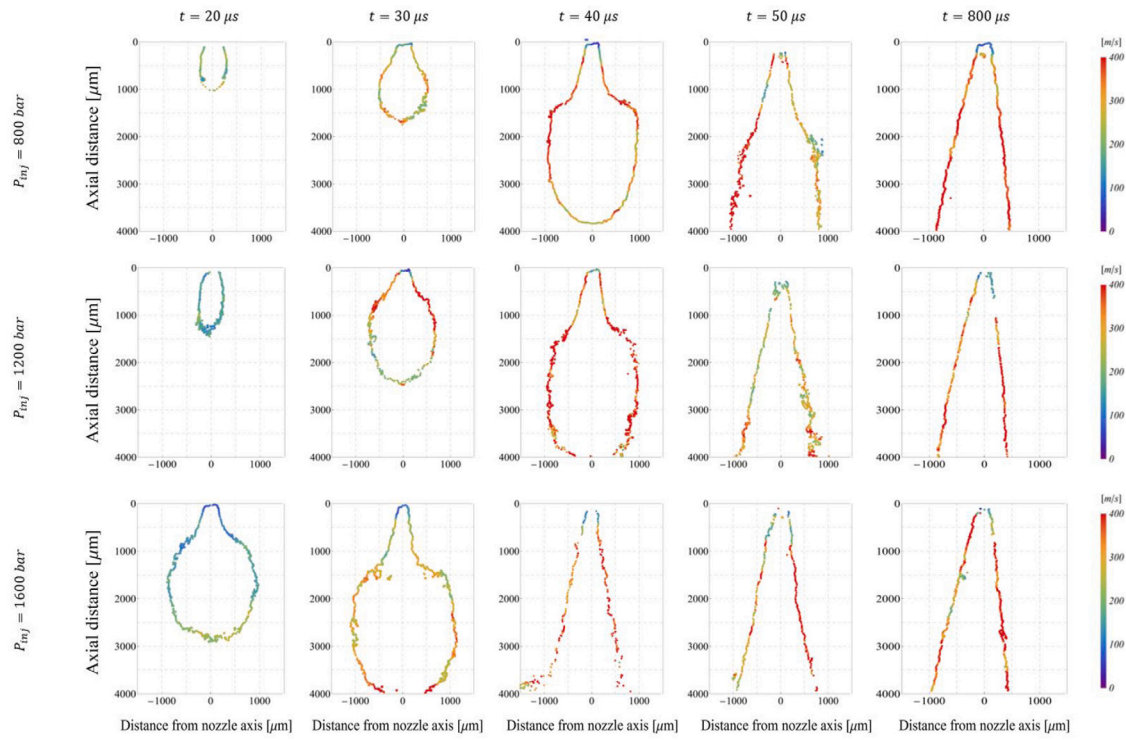
Fig. 7. Mean velocity magnitude for the off-axis nozzle over a range of pressures and timings. (For interpretation of the references to color in this figure legend, the reader is referred to the web version of this article.)

Fig. 8. Mean velocity magnitude for the TH-A orifice over a range of pressures and timings. (For interpretation of the references to color in this figure legend, the reader is referred to the web version of this article.)
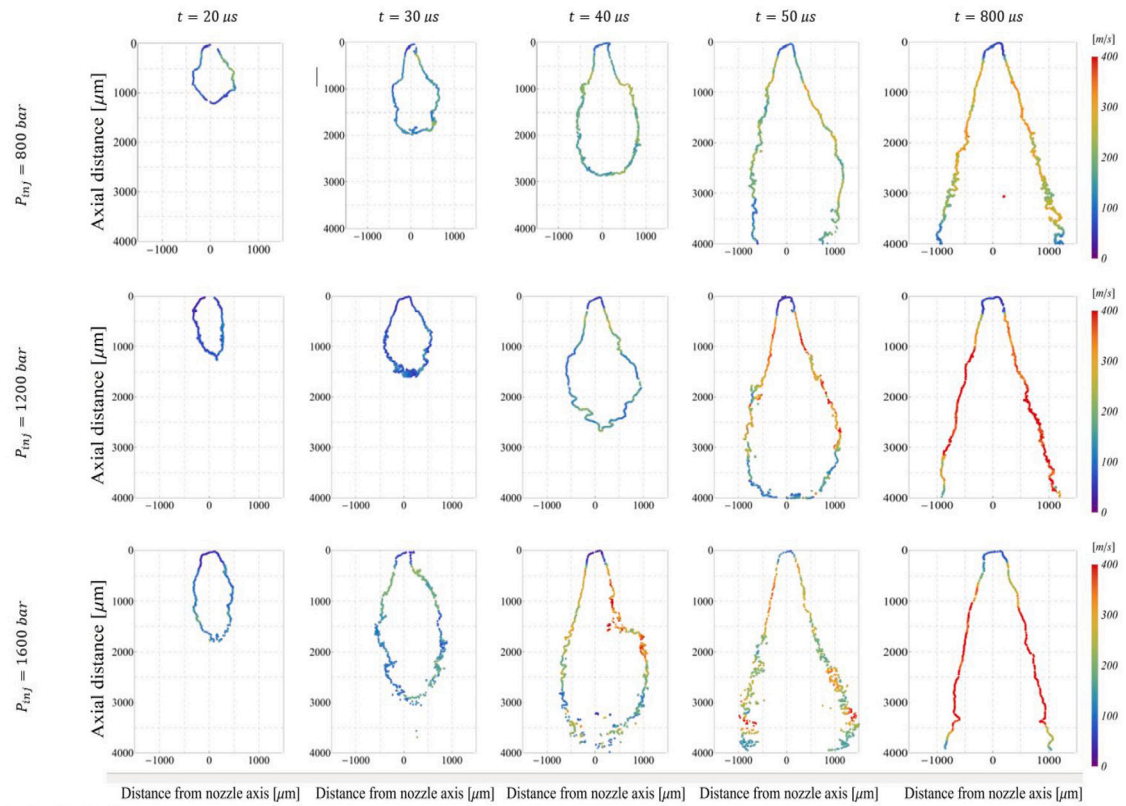
Fig. 9. Mean velocity magnitude for the TH-A orifice over a range of pressures and timings. (For interpretation of the references to color in this figure legend, the reader is referred to the web version of this article.)
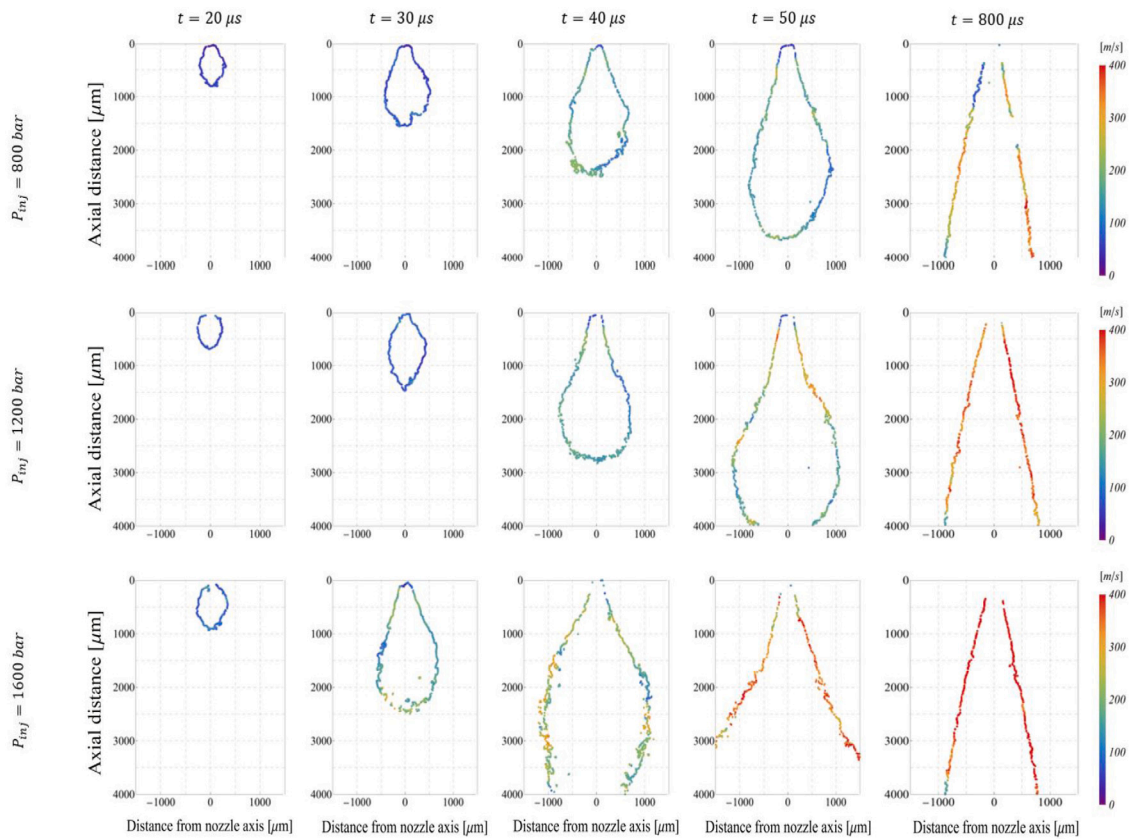
However, the results show that spray velocity increases on the left side at 3 mm from the nozzle tip, which happens for all three orifices. The deviation of the liquid core to the left side seems to transfer some energy to this spray region.

Unlike other nozzles, the spray of the SH nozzle is formed at a slower speed and is narrower in its shape. In this nozzle, there is no change in the direction of the internal flow as severely as in the other nozzles since there is no orifice inclination nor the asymmetry that exists in the OA nozzle. These two critical factors, and possibly the smaller diameter of the orifice, cause significant differences in spray behavior and velocity distribution for SH nozzle. Figs. 11 and 12 display the average radial and axial velocity distribution for the SH nozzle, respectively. These diagrams shows that the spray initially has a low axial velocity. However, the axial velocity gradually increases over time from the start of the injection. Radial velocities are very close to zero, which indicates a minimal amount of expansion in the radial direction of the spray. As stated earlier, we hypothesized the possible reason for the lower spray velocities in the TH nozzle, which is the larger cross-sectional area. Accordingly, we expected to see higher axial velocities in the spray of the SH nozzle. However, despite the smaller diameter of the SH orifice, the axial velocities of the spray are less than for the OA's. Analyses show that the SH nozzle's spray penetration is approximately equal to that of the OA. Thus, this indicates that the velocity of the liquid core is equal to or greater than the OA's spray centerline. Nevertheless, there seems to be more friction around the SH's orifice wall, which dissipates the flow energy on the spray periphery.

3.2. Spray development

The results show that the velocity is very low in the region close to the nozzle outlet, especially at the beginning of the injection. The flow accelerates within a short time after the start of injection and reaches a maximum relative value when it goes to the quasi-steady state (800 μs). Therefore, it is supposed that the initial velocity of the primary fuel portion that leaves the nozzle is close to zero just at the beginning of the injection, and the velocity at the orifice exit increases over time. This could be because as the needle lift increases, it creates a higher mass flow rate, meaning that the flow inside the injector cavity will accelerate for a few microseconds after the start of injection. Therefore, the fluid velocity exceeds the initial value when departing the nozzle at later time instants. It should be noted that this acceleration is referenced to the velocity changes of the same spray location over the next time stages. However, considering the same time instant, the velocity distribution is not uniform at different axial and radial coordinates. The results show that in the middle of the early transient phase (from 30 or 40 μs), the spray decelerates as it moves downward. However, at the beginning of the injection, the spray tip velocity appears higher than its upstream flow. As mentioned earlier and according to the injection rate diagrams in Fig. 13, the flow accelerates sharply in the first 50 μs of the injection. Therefore, the flow that comes out of the nozzle at 20 μs has a higher velocity than the flow that has been exited a few microseconds in advance. It seems that the momentum exchange between high-speed and low-speed flows leads to such velocity distribution during the transient startup of the injection event. Nevertheless, the leading edge slows down as the spray penetrates, which can have various reasons, such as induced drag force or the rise of instabilities. In addition, Tang et al. have also noticed a slight deceleration in spray tip penetration which they believe is caused by the break-up of a mushroom-shaped mass fraction [11]. Similarly, we can observe such a shape in the spray evolution pattern at the beginning of injection. As Crua et al. have identified [19], perhaps this fraction is a mixture of residual liquid fuel and gas trapped in the sac volume between the injections.
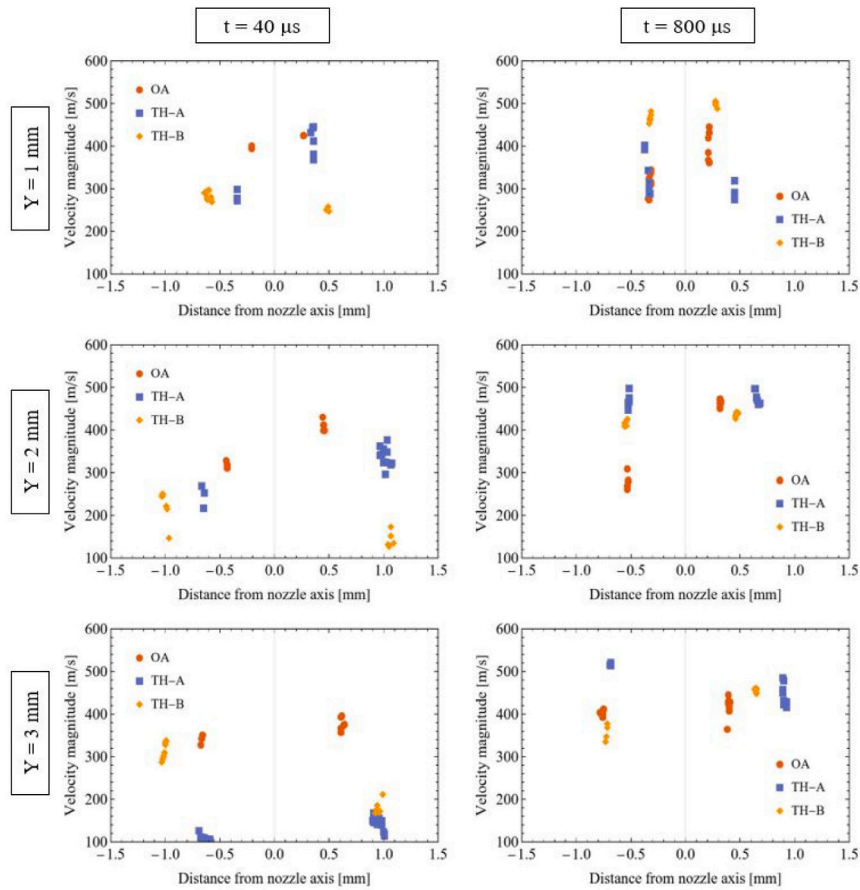
Fig. 10. Average velocity magnitude for OA and TH nozzles at specific axial locations and time-stages with the injection pressure of 1600 bar.
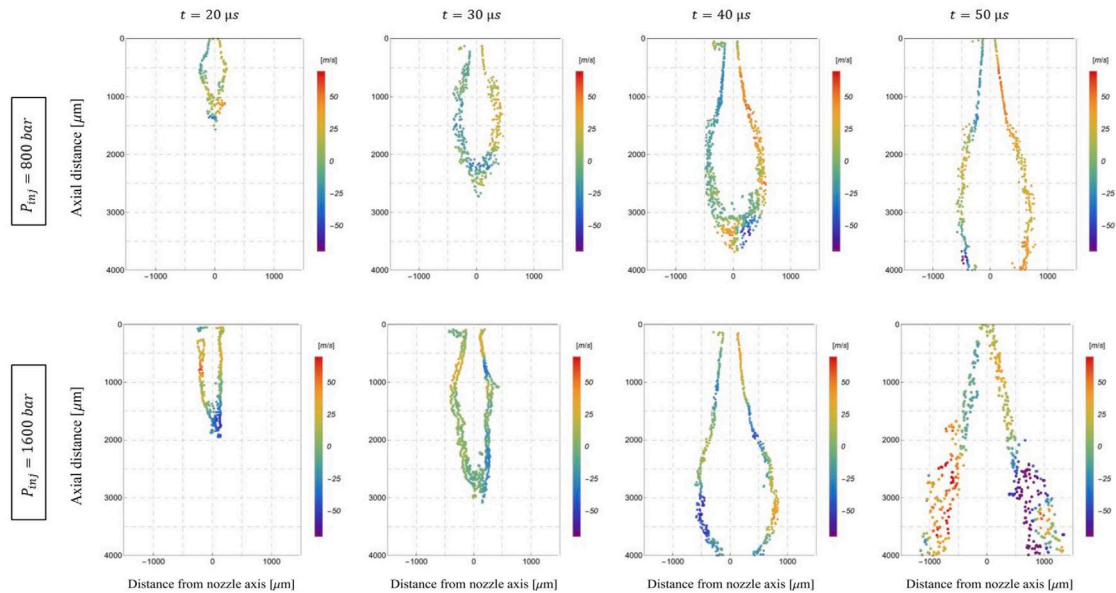

Fig. 11. Radial velocity distribution for single hole, on-axis orifice over two different injection pressures.

It seems that velocity differential at upstream and downstream could also contribute in forming the mushroom-shaped mass at the beginning of the injection. This mass forms and grows near the nozzle and travels downstream. The amount of surface expansion of this mass depends on the geometry of the nozzle, but the results show that it is not very sensitive to the injection pressure. Comparison of spray pro-files shows that the extent of this mass is the greatest in the OA nozzle, and the SH nozzle creates the least expansion. In addition, the growth rate of this mass is almost at the same level in both orifices of the TH nozzle. According to the geometry of these nozzles, it is presumed that
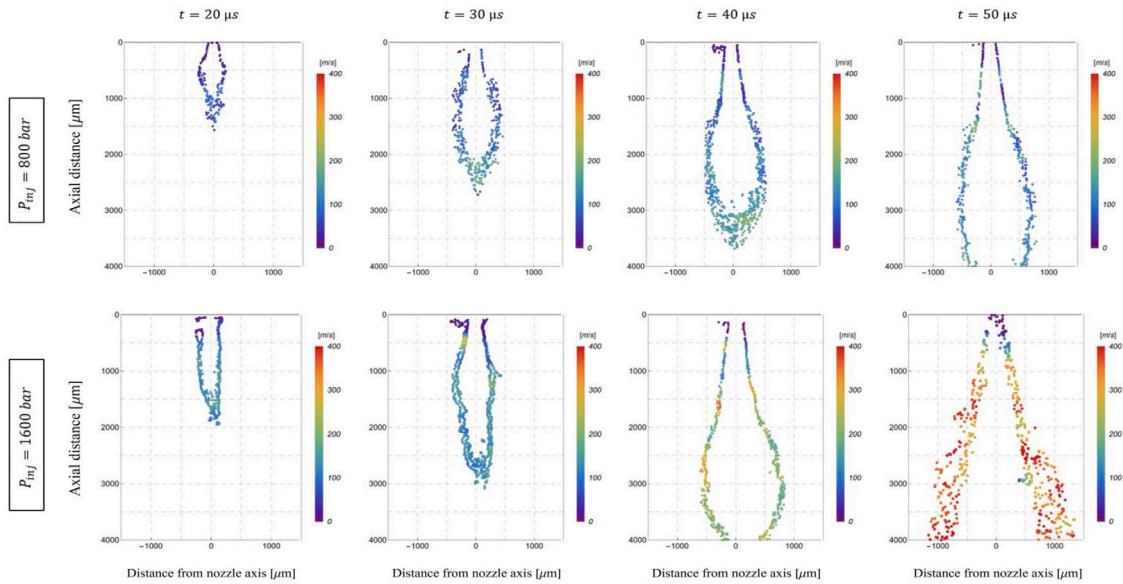
Fig. 12. Axial velocity distribution for single hole, on-axis orifice over two different injection pressures.
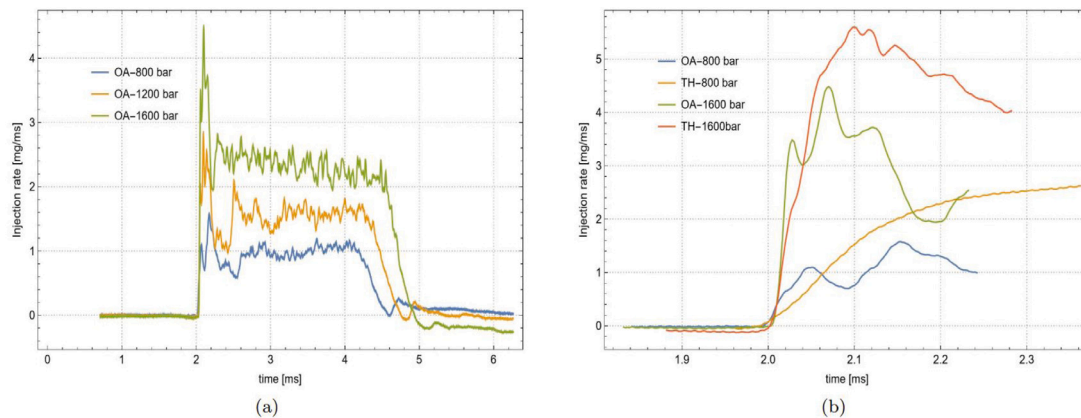

Fig. 13. Injection rate diagrams (a) for nozzle OA at three injection pressures and (b) for nozzle OA and TH just at the beginning of the injection.

they are mainly different potentials for generating cavitation. In addition, the internal flow streamline of each nozzle is distinct. However, since cavitation is associated with the injection pressure, thus cavitation cannot be the main reason for the formation of this mushroom-shaped mass; otherwise, the size of this mass should have changed significantly by increasing the injection pressure. Therefore, to find the root cause of the formation of this mass and the factors affecting it, we must pay attention to other factors, including the internal flow streamline.

According to Figs. 8 and 9, the formation of this mass is similar in both TH orifices but slightly different than other nozzles. For these orifices, an arc is formed on the right side of the spray. Inspection of orifice walls on the left and right sides of the spray shows that the flow on the right side exits slightly earlier than on the other side; the spherical outer surface of the nozzle created uneven orifice walls so that the right wall is shorter than the left one. In addition, at the orifice inlet, the left edge looks sharper. However, neither of these two points can explain such spray behavior reasonably because these features are also present in the OA nozzle, while no asymmetrical arc forms within the spray of this nozzle. Nevertheless, the main difference between the OA and TH nozzles is the inclination of the orifices from the injector axis. This inclination appears to create momentum in the flow, which leads to forming an arc on the right side of the spray. In both cases, the arc is formed on the lower wall, making this conclusion more sensible.

As mentioned earlier, the extent of the mushroom-shaped mass in the OA nozzle is the highest and formed differently from the other two nozzles. Analysis of velocity components in the radial direction expresses an outstanding behavior. As Fig. 14 shows, at the beginning of injection, the radial velocities on the right side of the spray are pointing towards positive values of the transverse axis, while on the other side velocities are negative, meaning that the mushroom-shaped mass volume expands to the sides. However, an interesting point arises in later time instants: at 30 and 40 μs radial velocity components at the top of this mass have an inverted direction while the bottom of this mass keeps the same radial velocity direction as at the beginning of injection. This process is independent of injection pressure, and according to Fig. 14, such a case is observable in all studied injection pressures. This result suggests that vortices are likely to form inside the mass fraction, creating a tumble that is reflected in the radial velocity profile. Assuming that the accelerating flow in the center of the spray penetrates into this mass at high relative velocity, it probably creates a relative vacuum inside the mass upstream which can be explained graphically by Fig. 15. However, the axial velocity of the liquid core and the mass downstream get synchronized. It is thought that this mechanism improve the air entrainment, but on the other hand, it induces a loss in the axial flow and impedes acceleration in the axial direction.
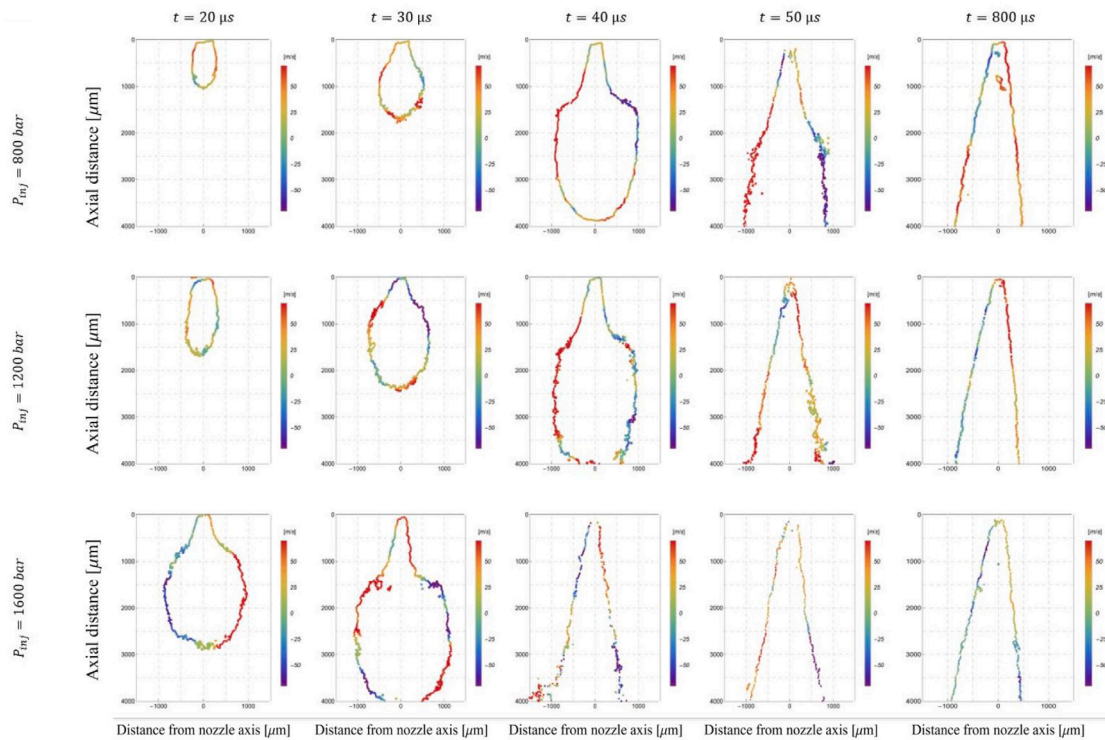
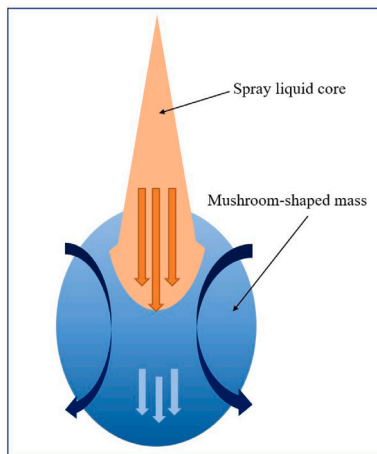**Fig. 14.** Radial velocity distribution for the off-axis nozzle over a range of pressures and timings.

Fig. 15. A graphical representation of the hypothesis of induced tumble in the mushroom-shaped mass by the spray liquid core.

3.3. Hole-to-hole variation

Studying the TH nozzle and its spray velocity distribution diagrams can provide information regarding hole-to-hole variation and interaction. In addition, that will help investigate the effect of orifice inclination. Analysis of eccentric needle movement addresses that sprays of a multi-hole injector are not identical, while their axial velocities fluctuate over the injection period. In other words, the dynamics of each spray fluctuate under a particular frequency, and that frequency is independent of injection pressure, and the number of holes [20]. According to this study, the primary cause of this fluctuation is the eccentric movement of the needle. In addition, since there is no phase lag in axial velocity oscillation, thus the variation in sac pressure is the main contributor to that matter rather than hole-to-hole variation. In the current study, since the TH nozzle has only two holes, the

sac pressure variation is expected to be less than the conventional injectors with nozzles of 8 to 12 holes. This study shows that the sprays of TH-A and TH-B undergo their unique evolutionary path, although both orifices have a similar rate of development. However, the radial velocities are higher in TH-B, which has led to a more significant radial expansion during the early transient phase as it is evident in Fig. 16. This behavior could be primarily due to the minor geometrical differences between orifices.

Moreover, due to the geometrical constraints of the chamber and injector fuel line, we had to mount the injector body diagonally. The angle between the injector axis and horizontal plane in this configuration becomes 21°. Consequently, the angle between the vertical axis and TH-A orifice will be 4° while this value is equal to 142° for the case of TH-B. Therefore, the fluid inside the nozzle experiences a more severe change in its direction to exit TH-B. This rotation in the flow direction induces centrifugal and centripetal forces on the spray periphery, which results in more spray expansion. In addition, with higher injection pressures, radial velocities also increase in both TH-A and TH-B orifices. It is evident by comparing sprays of TH-A and TH-B at 50 μs at every injection pressure.

Another point worth noting is the differences in average penetration and overall velocities in TH-A and TH-B cases. Comparing these sprays within the same time frame and pressure indicates that TH-B's overall velocity magnitude is slightly smaller at every injection pressure. A potential reason could be related to the installation angle of the injector body. As mentioned earlier, the internal flow is likely to experience more bends, which induces a loss in the flow. Therefore, we suspect that the injector orientation might contribute to hole-to-hole spray variation in multi-hole injectors. Hence, the installation angle is likely to influence the internal flow and the near-field spray velocity. We can easily verify this hypothesis in the future by rotating the injector by 180° and exchanging the position of each orifice. However, the minor geometrical differences between these orifices might also contribute to this matter.

Spray profiles in Figs. 7, 8 and 9 show another debatable issue; after 40 or 50 μs, the left side of the spray inclines towards the negative side
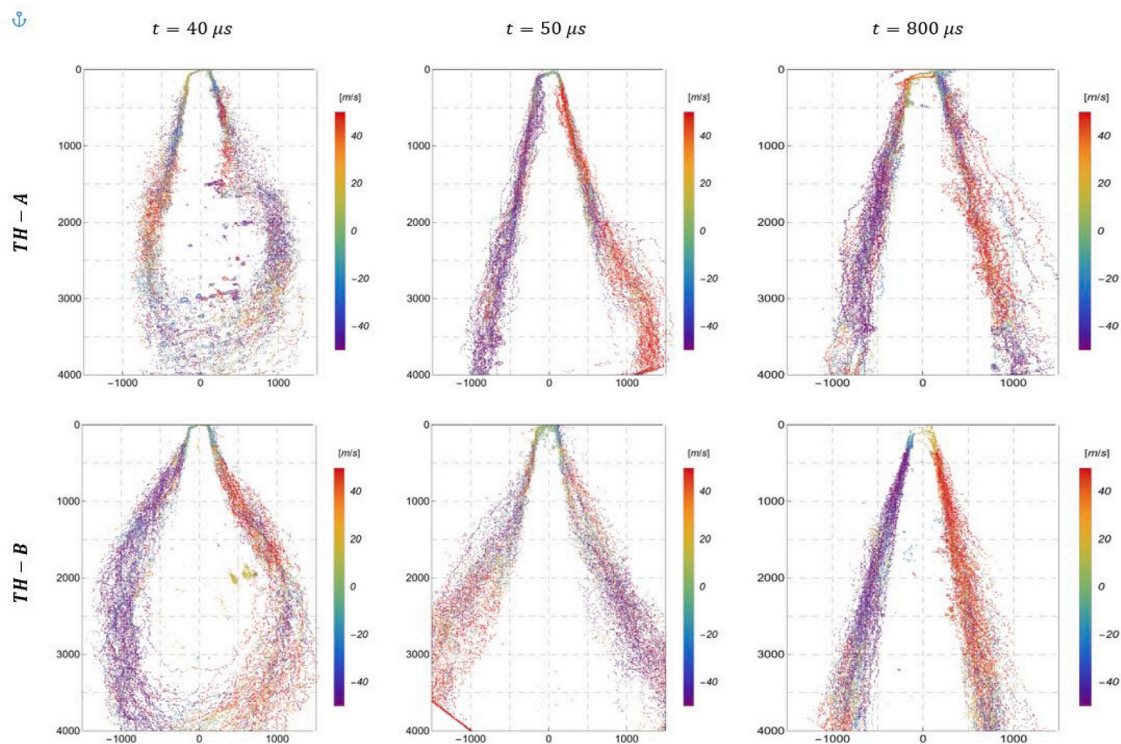
Fig. 16. Radial velocity distribution for the two-hole nozzle over a range of timings at 1600 bar injection pressure.

of the horizontal axis. In addition, the right side of the spray also tends to incline towards the left side and forms a small arc on the right side of the spray. Deviation towards the left side is even more evident in the quasi-steady state. Although this is not the case in orifice TH-A, it is visible in the other two orifices (OA and TH-B), regardless of injection pressure. In addition, the velocity profiles at 800 μs, indicate that the velocity magnitudes on the left side of the spray are lower than on the right side. It becomes more interesting when we realize that sharper orifice inlet edge is also located at the left side. Increasing the pressure seems to exacerbate this velocity asymmetry. Therefore, we expect that the increase in injection pressure boosts the deviation angle, although this change seems negligible according to the results. However, to find a more accurate answer in this regard, investigation in the far-field might be required.

3.4. Injection pressure

The injection pressure directly influences the timing of spray evolution because it reduces the nozzle opening delay and consequently shortens the transient phases. In addition, injection rate profiles in Fig. 13 show that the average injection rate at 800 bar is 1 mg/ms, increasing to 1.4 and 2.2 at 1200 bar and 1600 bar, respectively. Therefore the average velocity would increase significantly by injection pressure. However, as Fig. 17 depicts, the velocity magnitudes at spray periphery are just slightly higher at 1600 bar. This is in accordance with previous studies by Payri et al. [21], and Moon et al. [22] that have shown that the injection pressure mainly increases the velocity of the central spray and has the least influence at farther locations from the spray axis. Fig. 17 also shows an apparent velocity asymmetry on the opposite sides of the spray. This asymmetry increases by injection pressure so that the velocity of the left side of the spray, where there is a sharp edge at the orifice inlet, is higher at lower injection pressures. In other words, the sharp edge induces more significant losses as pressure increases.

Regarding the physical characteristics, the effect of pressure on the average spray profile is negligible at the quasi-steady state. We also

observed a similar spray evolution pattern during the early transient phase; however, these similar patterns appear at earlier time stages when pressure is higher. To clarify this statement, we can compare the average spray profile at 30 μs & 1600 bar with the one at 40 μs & 800 or 40 μs & 1200 bar. Nevertheless, overall velocity magnitudes are much different in these cases. In other words, comparing two cases with the same penetration length but different injection pressure, the velocity is higher in the case with higher pressure. Therefore, higher injection pressure raises the spray acceleration during the early transient phase. On the other hand, the nozzle opening delay becomes smaller with pressure rise, indicating a higher acceleration of needle motion. Therefore, one can conclude that the spray acceleration is primarily a function of the needle acceleration in the transient phase. However, the overall force acting on the needle is proportional to the injection pressure; thus, increasing the injection pressure transforms into a higher acceleration in the needle.

The analysis of the effect of injection pressure on TH-A and TH-B shows a surprising point. As Figs. 8 and 9 depict that velocities and penetration at 1200 bar are unexpectedly lower or relatively equal to the 800 bar condition. This effect is less likely to result from error or accident because we performed the image acquisition for each time instant/pressure over different days with the same setup. Nevertheless, by increasing the injection pressure to 1600 bar, the flow accelerates and penetration at respective time instants improves. In near-field spray evolution, there might be a critical injection pressure so that the turbulent interactions and instabilities suppress the growth in spray velocity. However, elevating the injection pressure beyond that critical value would overcome the losses induced. By the way, to justify this hypothesis, we need more statistics. In addition, the nozzles' internal flow characteristics can also provide a window to the correct answer. In addition, it should be noted that these experiments were conducted in ambient conditions. Payri et al. [21] show that increasing the density will reduce the spray velocities non-linearly. However, its effect on the outer spray surface seems insignificant, similar to the effect of injection pressure.
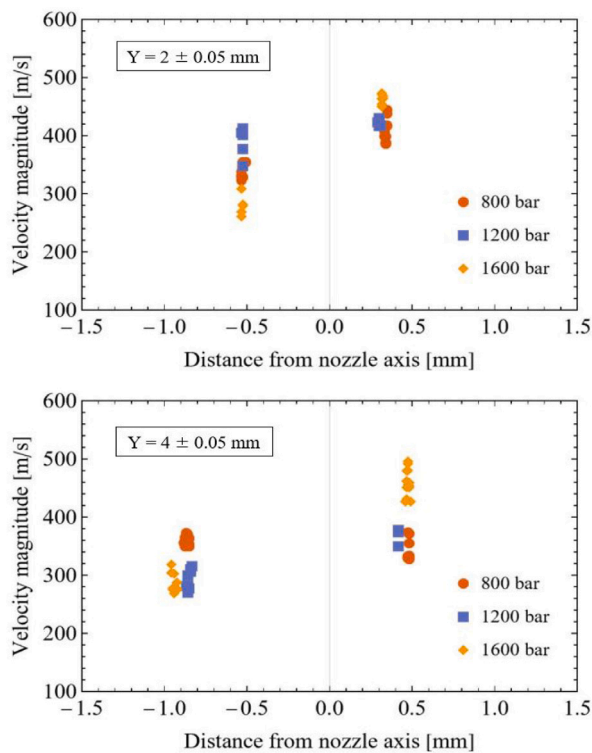
Fig. 17. Average velocity magnitude at specific axial distances (Y ± 0.05 mm) from the nozzle tip for nozzle OA at 800 μs ASOI.

4. Conclusion

This study visualized the kinematics of near-field diesel spray for asymmetrical nozzle geometries. In this study, we measured and collected velocity information for 45 sprays in total, which belong to three orifices, three injection pressures, and five time-instants. In addition, more than 150 image pairs were taken and processed for each of these sprays to statistically investigate the effect of asymmetrical orifice inlet on the spray kinematics. We also have shown that the calculated mean velocities are convergent with 95% certainty and the maximum confidence interval is ±18 m/s.

The results show that the spray of the single-hole off-axis nozzle moves faster than for both orifices of the two-whole nozzle. In addition, injection rates of the whole two-hole nozzle are lower than the single-hole off-axis nozzle up to the 50 μs after the start of injection. However, they show less significant velocity differences as the needle lift increases and the flow reaches a quasi-steady state. Since the outlet cross-sectional area of the two-hole nozzle is 1.6 times larger than the off-axis one, we suspect that initial velocity in a multi-hole injector will be reduced by increasing the number of holes, even though the injection rate of the nozzle is increased.

Regarding the general spray development, we observed in all cases that the spray periphery has a near zero velocity just after the hydraulic start of injection. This initial low-velocity is probably because the first portion of the fuel exiting the orifice often contains residual fuel and air trapped in the sac volume from the previous injection. Since the velocity of the residuals is close to zero, they lead to slight resistance against the fresh incoming flow. However, as the needle rises further, the momentum and velocity of the flow increase, causing the spray acceleration for a few microseconds depending on the injection pressure. The acceleration is due to mixing and momentum exchange with the upcoming flow. However, velocity magnitudes become smaller at downstream due to energy dissipation shortly after that.

At the same time frame, a fraction of fuel is formed, which resembles a mushroom shape. Analyzing the radial velocity components shows that the upstream parts of this mass fraction are moving towards the spray center while the downstream part is expanding. This condition suggests that a circular motion is created when the upstream flow – which is moving faster – mixes with the slow-moving flow, which has been exited at an earlier time stage.

In the case of asymmetrical inlet geometry, the average spray axis deviates from the center towards the side with a sharper orifice inlet edge. This phenomenon is more remarkable for the off-axis nozzle and will affect spray targeting. In addition, the velocity distribution is not symmetrical on the two opposite sides of the spray. As injection pressure increases, losses will become more significant on the side with a sharp edge, and thus velocities become less than measured values at lower injection pressures. Therefore, the restrictions to the flow by sharp orifice will become more significant as the injection pressure rises. According to this study, velocity asymmetry grows linearly by injection pressure. Accordingly, increasing the injection pressure reduces the velocity at the side with a sharp orifice edge as much as the velocity increases on the other side.

Finally, the injection pressure impacts nozzle opening delay and can increase the needle acceleration, directly affecting spray acceleration and evolution. Therefore, higher injection pressure reduces the time for spray evolution by increasing the flow's velocity and acceleration and shortening the transient phase by accelerating the needle movement. However, in this study, injection pressure does not influence the overall spray profile. In addition, although the injection rate increases linearly by pressure, the velocity at the spray periphery increases marginally.

CRediT authorship contribution statement

Mohammad Nikouei: Writing – original draft, Writing – review & editing, Visualization, Investigation, Software, Methodology, Data curation. **David Sedarsky:** Conceptualization, Methodology, Software, Validation, Writing – review & editing, Supervision, Funding acquisition, Resources, Project administration.

Declaration of competing interest

The authors declare that they have no known competing financial interests or personal relationships that could have appeared to influence the work reported in this paper.

Data availability

Data will be made available on request.

References

[1] Du W, Lou J, Yan Y, Bao W, Liu F. Effects of injection pressure on diesel sprays in constant injection mass condition. Applied Thermal Engineering 121:234–41, http://dx.doi.org/10.1016/j.applthermaleng.2017.04.075 URL https://www.sciencedirect.com/science/article/pii/S1359431116340686.

[2] Hawi M, Kosaka H, Sato S, Nagasawa T, Elwardany A, Ahmed M. Effect of injection pressure and ambient density on spray characteristics of diesel and biodiesel surrogate fuels. Fuel 254:115674, http://dx.doi.org/10.1016/j.fuel.2019.115674 URL https://www.sciencedirect.com/science/article/pii/S0016236119310269.

[3] Salvador FJ, Gimeno J, De la Morena J, González-Montero LA. Experimental analysis of the injection pressure effect on the near-field structure of liquid fuel sprays. Fuel 292:120296, http://dx.doi.org/10.1016/j.fuel.2021.120296 URL https://www.sciencedirect.com/science/article/pii/S0016236121001721.

[4] Wang Z, Jiang C, Xu H, Wyszynski ML. Macroscopic and microscopic characterization of diesel spray under room temperature and low temperature with split injection. Fuel Processing Technology 142:71–85, http://dx.doi.org/10.1016/j.fuproc.2015.10.007 URL http://www.sciencedirect.com/science/article/pii/S0378382015301946.

[5] Desantes JM, García-Oliver JM, Xuan T, Vera-Tudela W. A study on tip penetration velocity and radial expansion of reacting diesel sprays with different fuels. Fuel 207:323–35, http://dx.doi.org/10.1016/j.fuel.2017.06.108 URL https://www.sciencedirect.com/science/article/pii/S0016236117308177.

[6] Payri R, Viera JP, Gopalakrishnan V, Szymkowicz PG. The effect of nozzle geometry over internal flow and spray formation for three different fuels. Fuel 183:20–33, http://dx.doi.org/10.1016/j.fuel.2016.06.041 URL https://www.sciencedirect.com/science/article/pii/S0016236116304938.

[7] Du C, Andersson M, Andersson S. Effects of nozzle geometry on the characteristics of an evaporating diesel spray. SAE Internationa Journal of Fuels and Lubricants 9(3):493–513, http://dx.doi.org/10.4271/2016-01-2197 URL https://www.sae.org/publications/technical-papers/content/2016-01-2197/?PC=DL2BUY.

[8] Yao C, Geng P, Yin Z, Hu J, Chen D, Ju Y. Impacts of nozzle geometry on spray combustion of high pressure common rail injectors in a constant volume combustion chamber. Fuel 179:235–45, http://dx.doi.org/10.1016/j.fuel.2016.03.097 URL https://www.sciencedirect.com/science/article/pii/S0016236116301399.

[9] Yu S, Yin B, Deng W, Jia H, Ye Z, Xu B, Xu H. Experimental study on the spray characteristics discharging from elliptical diesel nozzle at typical diesel engine conditions. Fuel 221:28–34, http://dx.doi.org/10.1016/j.fuel.2018.02.090 URL https://www.sciencedirect.com/science/article/pii/S0016236118302497.

[10] Salvador FJ, Carreres M, Jaramillo D, Martínez-López J. Analysis of the combined effect of hydrogrinding process and inclination angle on hydraulic performance of diesel injection nozzles. Energy Conversion and Managemen 105:1352–65, http://dx.doi.org/10.1016/j.enconman.2015.08.035, URL https://www.sciencedirect.com/science/article/pii/S0196890415007815.

[11] Tang C, Feng Z, Zhan C, Ma W, Huang Z. Experimental study on the effect of injector nozzle k factor on the spray characteristics in a constant volume chamber: Near nozzle spray initiation, the macroscopic and the droplet statistics. Fuel 202:583–94, http://dx.doi.org/10.1016/j.fuel.2017.04.078 URL https://www.sciencedirect.com/science/article/pii/S0016236117305033.

[12] Payri R, Salvador FJ, De la Morena J, Pagano V. Experimental investigation of the effect of orifices inclination angle in multihole diesel injector nozzles. Part 2 – spray characteristics. Fuel 213:215–21, http://dx.doi.org/10.1016/j.fuel.2017.07.076 URL https://www.sciencedirect.com/science/article/pii/S0016236117309389.

[13] Zama Y, Odawara Y, Furuhata T. Experimental investigation on velocity inside a diesel spray after impingement on a wall. Fuel 203:757–63, http://dx.doi.org/10.1016/j.fuel.2017.04.099 URL https://www.sciencedirect.com/science/article/pii/S0016236117305252.

[14] Sedarsky D, Idlahcen Sd, Blaisot J-B, Rozé C. Velocity measurements in the near field of a diesel fuel injector by ultrafast imagery. Experiments in Fluids 54(2):1451, arXiv:1301.6593 http://dx.doi.org/10.1007/s00348-012-1451-9 URL http://arxiv.org/abs/1301.6593.

[15] Cao Z-M, Nishino K, Mizuno S, Torii K. PIV measurement of internal structure of diesel fuel spray. Experiments in Fluids 29:S211–9, http://dx.doi.org/10.1007/s003480070023.

[16] Linne MA, Paciaroni M, Berrocal E, Sedarsky D. Ballistic imaging of liquid breakup processes in dense sprays. Proceedings of the Combustion Institute 32(2):2147–61, http://dx.doi.org/10.1016/j.proci.2008.07.040 URL https://www.sciencedirect.com/science/article/pii/S1540748908000308.

[17] Purwar H, Idlahcen Sd, Rozé C, Sedarsky D, Blaisot J-B. Collinear, two-color optical Kerr effect shutter for ultrafast time-resolved imaging. Optics Express 22(13):15778, arXiv:1502.03350 http://dx.doi.org/10.1364/OE.22.015778 URL http://arxiv.org/abs/1502.03350.

[18] Yan F, Du Y, Wang L, Tang W, Zhang J, Liu B, Liu C. Effects of injection pressure on cavitation and spray in marine diesel engine. International Journal of Spray and Combustion Dynamics 9(3):186–98, http://dx.doi.org/10.1177/1756827716672472 URL https://doi.org/10.1177/1756827716672472.

[19] Crua C, Heikal MR, Gold MR. Microscopic imaging of the initial stage of diesel spray formation. Fuel 157:140–50, http://dx.doi.org/10.1016/j.fuel.2015.04.041 URL https://www.sciencedirect.com/science/article/pii/S0016236115004391.

[20] Huang W, Moon S, Gao Y, Li Z, Wang J. Eccentric needle motion effect on near-nozzle dynamics of diesel spray. Fuel 206:409–19, http://dx.doi.org/10.1016/j.fuel.2017.06.012 URL http://www.sciencedirect.com/science/article/pii/S0016236117307032.

[21] Payri R, Viera JP, Wang H, Malbec L-M. Velocity field analysis of the high density, high pressure diesel spray. International Journal of Multiphase Flow 80:69–78, http://dx.doi.org/10.1016/j.ijmultiphaseflow.2015.10.012 URL https://www.sciencedirect.com/science/article/pii/S0301932215002542.

[22] Moon S, Gao Y, Wang J, Fezzaa K, Tsujimura T. Near-field dynamics of high-speed diesel sprays: Effects of orifice inlet geometry and injection pressure. Fuel 133:299–309, http://dx.doi.org/10.1016/j.fuel.2014.05.024 URL https://www.sciencedirect.com/science/article/pii/S0016236114004712.